Inorg. Chem., **14**, 417 (1975).
(3) J. M. Fruchart, G. Herve, J. P. Launay, and R. Massart, *J. Inorg. Nucl. Chem.*, **38**, 1627 (1976).
(4) H. Wu, *J. Biol. Chem.*, **43**, 189 (1920).
(5) A. Tézé and G. Hervé, *J. Inorg. Nucl. Chem.*, **39**, 999 (1977).
(6) P. Souchay, "Ions Mineraux Condensés", p. 93, Masson et Cie, Paris, 1969.
(7) H. K. Saha and A. K. Banerjee, *Inorganic Syntheses*, **15**, 100 (1974).
(8) H. So and M. T. Pope, *Inorg. Chem.*, **11**, 1441 (1972).
(9) G. Lange, H. Hahn, and K. Dehnicke, *Z. Naturforschg.*, **24b**, 1498 (1969).
(10) C. Roccicioli-Deltcheff and R. Thouvenot, *J. Chem. Res. (M)*, 0549 (1977).
(11) C. Sanchez, J. Livage, J. P. Launay, M. Fournier and Y. Jeannin, *J. Amer. Chem. Soc.*, **104**, 3194 (1982).
(12) C. R. Hare, I. Bernal and H. B. Gray, *Inorg. Chem.*, **1**, 831 (1962).
(13) H. So, M. Kolor, P. R. Robinson, G. P. Haight, Jr. and R.L. Belford, *J. Coord. Chem.*, **9**, 43 (1979).
(14) T. Imamura, G. P. Haight, Jr., and R. L. Belford, *Inorg. Chem.*, **15**, 1074 (1976).
(15) Our unpublished results.
(16) Reference 6, p. 97.
(17) However, the isosbestic point that appears during the evolution of Spectrum A is less clearly seen at this pH. Moreover, the stable isomer of $[PMoW_{11}O_{40}]^{4-}$ is believed to disproportionate at pH $\geq$ 2. See Reference 2. These are the reasons why we present the spectra at pH 1.1 in Figures 1 and 2.
(18) The molybdenum complexes that contribute to Spectrum A at 20.2 kK and their molar absorptivities are Complex A ($\varepsilon > 3040$), Complex B(ε 980), and $[Mo_2O_4(PW_{11}O_{39})_2]^{12-}$ ($\varepsilon/2 < 170$ dm^3 mol^{-1} cm^{-1}). The last complex is discussed later in the text.

MO Theoretical Studies on the Effect of Bond Angle Distortion in Pyrazine

Ikchoon Lee† and Ho Soon Kim

Department of Chemistry Inha University, Incheon 160, Korea (*Received November 10, 1983*)

An enhancement of through-bond interaction by bond angle distortion in pyrazine was examined using various MO methods. Results of MINDO/3 geometry optimization with an angle (α) at C_2 atom fixed to 120~90° lead to distorted structures in which the distorted bond is brought closer toward lone pair orbital n of N atom. It was also found that the bond angle distortion increased the P character at the atom C_2, resulting in an increased vicinal overlap between n and the C_2–C_3 bond. The FMO patterns of σ framework showed three-fold degeneracy, one of which was of different symmetry which mixes in the symmetry adapted pair, n_+ and n_-; both n_+ and n_- orbitals thus can interact with both FMOs of the σ framework. The LCBO-MO analysis with partial elimination of bonds, antibonds or both, however, revealed that the main interaction of n_+ was with the HO-σ and that of n_- was with the LU-σ^* orbital of the σ framework.

Introduction

According to the perturbation molecular orbital (PMO) theory of orbital interactions[1], through-space (TSI) and through-bond interaction (TBI) energies of two nonbonding orbitals, n_1 and n_2, are obtained as first order and second order perturbation energy terms respectively. It has been shown[1] that the evaluation of second order (TBI) terms is simplified since interaction of the symmetry adapted pair, $n_+ = n_1 + n_2$ and $n_- = n_1 - n_2$, with one of the frontier MOs (FMO) always vanishes because of different symmetries involved in the two interacting orbitals depending on the number, N, of the intervening σ bonds, as summarized in Table 1. This has been succinctly demonstrated using FMO patterns of the σ-framework obtained based on the "C-approximation".

Recently it has been shown in a spectroscopic study of a cyclobutapyrazine derivative (I) that TBI of the two nitrogen lone-pair orbitals is enhanced due to distortion of bond angles at carbons 2 and 3 of pyrazine ring (II)[2].

This has been ascribed to an enhancement of the P character of the σ bond orbital through which the interaction occurs.

In this work we have carried out detailed analysis of the enhanced TBI due to bond angle distortion using pyrazine as a model within the framework of PMO theory of orbital interactions.

TABLE 1: Through-bond Interaction Schemes between $n_\pm$ and FMOs of σ-framework

symmetry adapted pair	framework σ-FMO			
	N=odd		N=even	
	HO-σ (S)	LU-σ^* (A)	HO-σ (A)	LU-σ^* (S)
n_+ (S)	y	0	0	$-x$
n_- (A)	0	$-x$	y	0

S and A refer to symmetric and antisymmetric orbitals respectively. X and y are the second order energy terms which are positive with $y > x$.

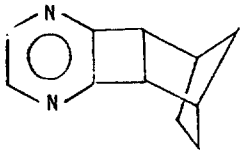

(I) *endo*-3,4-pyrazinotricyclo [4.2.1.$0^{2,5}$]nonane

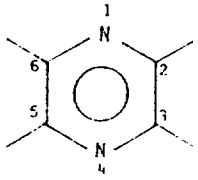

(II) Pyrazine

Computations

Geometries of various pyrazine structures were optimized with the MINDO/3 method[3] and the linear-combination-of-bond-orbitals (LCBO) calculations[4] at the CNDO level were used to carry out the bond (σ)-antibond (σ^*) analysis of orbitals. *Ab initio* (STO-3G) calculations[5] have also been performed using the MINDO/3 optimized geometries.

Results and Discussion

The bond angle α in pyrazine was independently varied from 120° to 90° and for a fixed value of α, the other geometries were optimized.

The results summarized in Table 2 indicate that the effects of decreasing α are: bond angle β increases whereas γ decreases, and bond lengths b and d decrease while a and c increase. The fully distorted structure can be represented as III.

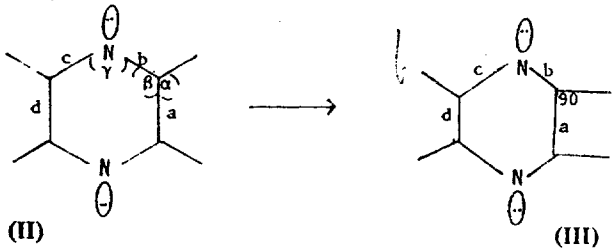

(II) (III)

Energy levels of n_+ and n_- calculated with three different methods using MINDO/3 geometries are summarized in Table 3, where the P character of the carbon 2 and S character of the lone pair in the n_+ orbital are also included.

The n_- level is in every case below n_+ in accordance with the expectation from the odd number (N) of the intervening C-C bonds[1]. Reference to Table 3 reveals that irrespective of the method of computation, bond angle (α) distortion induces further depression of n_- and elevation of n_+ levels. It is also seen from this table that these changes are accompanied with an increase in the P character of the carbon 2 and with a relatively small decrease in the S character of the lone pair orbital[2,6].

Vicinal overlap integrals S[7] between n and bond, σ, and antibond, σ^*, orbitals of a and d are given in Table 4.

Absolute values of S tend to increase for the overlap between n and a, $|Sna|$ and $|Sna^*|$, while those for the overlap between n and d, $|Snd|$ and $|Snd^*|$, tend to decrease, although the decrease in the latter is seen to be much smaller than the increase in the former.

Data in the Table 3, 4 and 5 are of course inter-related. Optimized geometries have shown that n and a are brought closer while n and d become farther apart as the angle α is decreased; natural consequences are the increase in $|Sna|$ and the relatively small decrease in $|Snd|$, which in turn will result in the enhanced TBI. The enhanced P character of the carbon 2 will also contribute to the increase in $|Sna|$ and hence in TBI[2,6(c)].

Energy splitting, $\Delta E=\varepsilon_+-\varepsilon_-$, energy change, $\delta\varepsilon=\varepsilon_{av}-\varepsilon_0$,

TABLE 2: MINDO/3 Optimized Geometries of Pyrazine with Fixed Bond Angle α

α	β	γ	a	b	c	d
120	120.7	118.5	1.409	1.335	1.335	1.409
105	122.2	115.6	1.433	1.321	1.349	1.405
95	123.2	113.3	1.460	1.313	1.361	1.399
93	123.2	113.2	1.466	1.311	1.362	1.398
90	123.2	113.1	1.479	1.308	1.364	1.395
90*	124.4	112.2	1.400*	1.327	1.350	1.411

*The bond-length a is fixed to 1.400Å arbitrarily.

TABLE 3: Changes in Energy Levels of n_+ and n_- Orbitals and in the S and P Characters as α is Changed

	α	orbital energy (eV)		S-character*	P-character*
		ε_-	ε_+		
MINDO/3	120	−9.940	−7.778	0.210	0.256
	105	−10.127	−7.709	0.206	0.296
	95	−10.242	−7.648	0.205	0.324
	93	−10.231	−7.610	0.204	0.329
	90	−10.219	−7.559	0.203	0.338
	(90*)	−10.111	−7.672	0.205	0.324
STO-3G	120	−11.209	−8.598	0.321	0.247
	105	−11.560	−8.543	0.308	0.284
	90	−11.786	−8.310	0.292	0.326
LCBO	120	−16.423	−12.169		
	105	−16.785	−12.050		
	90	−17.038	−11.740		

*AO coefficients for n_+ level.

where $\varepsilon_{av}=(\varepsilon_+ + \varepsilon_-)/2$ and splitting ratio, $SR=\frac{\varepsilon_0-\varepsilon_-}{\varepsilon_+-\varepsilon_0}$, are summarized in Table 5.

Very small TSI involved (*vide infra*) in pyrazine due to the long distance between the two n orbitals makes the magnitudes of these quantities eligible as measures of TBI. Inspection of Table 5 reveals that the magnitudes of these quantities and hence TBI increase with the degree of bond angle (α) distortion. We note that the enhancement of TBI is greater when both sides are subjected to bond angle distortion (group B), while introduction of a fused three membered ring on one side causes some reduction in TBI, (group C).

In the LCBO-MO method[4], MOs Ψ_i are constructed as a linear combination of "bonds, σ," "antibonds, σ^*," and "lone pairs, n," which are in turn formed by the directed hybrid orbitals of sp^3 and sp^2 types.

$$\Psi_i=\sum c_{ij}\, n_j+\sum c_{ik}\, \sigma_k+\sum c_{il}\, \sigma_l^* \qquad (1)$$

It is useful in this method to see what effect does the σ or σ^* have on the MO Ψ by eliminating a part of or the whole of σ or σ^* orbitals from the molecule. This type of technique was found useful especially in elucidating the importance of σ^* orbitals in conformational problems[8].

In order to gain further information as to the effect of bond angle distortion on TBI of two n orbitals in pyrazine, we considered six structures (B)~(G), in which σ or σ^* or both are eliminated from a part of the molecule as indicated by dotted line in Figure 1.

TABLE 4: Vicinal Overlaps between n and Bonds σ and Antibonds σ^* of α and d Calculated with LCBO-MO Method

α	S			
	Sna	*Sna**	*Snd*	*Snd**
120	−0.095	0.063	−0.095	−0.062
105	−0.100	0.069	−0.091	−0.059
90	−0.106	0.076	−0.086	−0.056

The level changes and energy splittings of the symmetry adapted pair, n_+ and n_-, accompanied by these partial deletion[9] are summarized in Table 6.

Three calculations for each structure in Figure 1 were performed: (i) with all bonds, σ, eliminated, (ii) with both bonds and antibonds, σ^*, eliminated, and (iii) with all antibonds eliminated, from the part concerned.

The structure A has no part deleted but considers two cases of bond angle α, 120° and 90°. It is seen from the Table 6 that bond angle distortion leads to depression of n_- level (0.59 eV) more than to raise n_+ level (0.43 eV).

In the structure B the two environment adjusted lone pairs are removed entirely from the rest of the molecule. As a result of distortion, the level of the HO-σ orbital of the σ framework is seen to be slightly elevated relative to that for the undistorted structure. This seems to be in line with the enhanced interaction (TBI) with the n_+ level due to

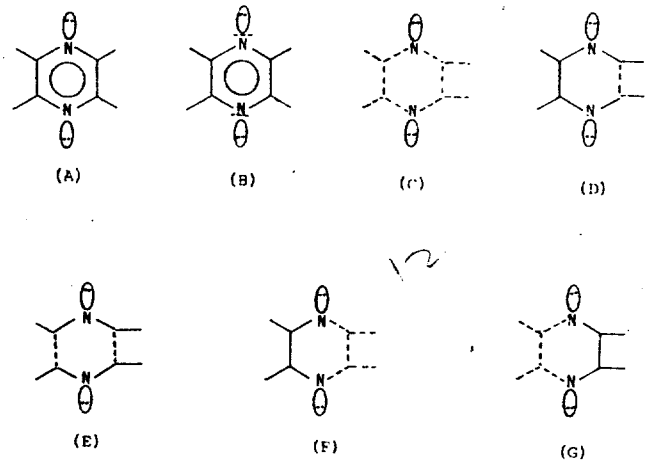

Figure 1. Undistorted, A and B with $\alpha=120$, and distorted, A and B with $\alpha=90$ and (B)-(G), structures with partially eliminated regions shown (·····).

TABLE 5: Energy Splitting $\Delta E=\varepsilon_+-\varepsilon_-$ (eV), Interaction Energy Change, $\delta\varepsilon=\varepsilon_{av}-\varepsilon_0$ (eV), and Splitting Ratio (SR)

		α	ΔE	ε_{av}	ε_0	$\delta\varepsilon$	SR
MINDO/3	A	120	2.17	−8.86	−8.43	−0.43	2.3
		105	2.42	−8.92	−8.39	−0.53	2.5
		95	2.59	−8.95	−8.35	−0.60	2.7
		93	2.62	−8.92	−8.32	−0.61	2.7
		90	2.66	−8.89	−8.27	−0.62	2.8
	B	120	2.17	−8.86	−8.43	−0.43	2.3
		105	2.63	−9.04	−8.44	−0.60	2.7
		90	3.00	−9.09	−8.36	−0.73	2.9
	C	120	3.08	−8.73	−7.83	−0.90	3.8
		105	3.16	−8.89	−7.98	−0.91	3.8
		90	3.16	−8.96	−8.09	−0.87	3.4
	D	di-CH_3	2.23	−8.65	−8.14	−0.51	2.7
STO-3G	E	120	2.61	−9.90	−9.04	−0.86	4.9
		105	3.02	−10.05	−9.03	−1.02	5.2
		90	3.48	−10.05	−8.84	−1.21	5.5

Gorup A: One side distorted. B: Both sides distorted. C: One side has a fused three membered ring. D: 2,3-Dimethyl pyazine. E: One side distorted.

TABLE 6: Energy Levels of n_+ and n_- and Energy Splirgy Splittings for Various Partially Eliminated Structures

			ε_-	ε_+	ΔE
A	$\alpha=120$		−16.44	−12.19	4.25
	$\alpha=90$		−17.03	−11.76	5.27
B	$\alpha=120$		HO—σ=−15.13		
	$\alpha=90$		HO—σ=−14.53		
	deleted orbital				
C	(i)	σ	−20.63	−20.44	0.19
	(ii)	$\sigma+\sigma^*$	−19.92	−20.11	−0.19
	(iii)	σ^*	−16.33	−11.35	4.98
D	(i)	σ	−17.03	−14.18	2.85
	(ii)	$\sigma+\sigma^*$	−16.79	−14.18	2.61
	(iii)	σ^*	−16.79	−11.76	5.03
E	(i)	σ	−17.03	−17.69	−0.66
	(ii)	$\sigma+\sigma^*$	−16.60	−17.69	−1.09
	(iii)	σ^*	−16.60	−11.76	4.84
F	(i)	σ	−17.31	−15.24	2.07
	(ii)	$\sigma+\sigma^*$	−16.65	−15.05	1.60
	(iii)	σ^*	−16.74	−11.65	5.09
G	(i)	σ	−17.12	−13.69	3.43
	(ii)	$\sigma+\sigma^*$	−16.93	−13.69	3.54
	(iii)	σ^*	−16.68	−11.46	5.22

the energy gap narrowing.

In the structure C, lone pairs are attached to N atoms but N atoms are cut off from the molecule in the three ways, *i.e.*, (i), (ii) and (iii), as classified above. First of all, in the case (ii), we have the situation where only TSI is possible between the two n orbitals. The results are as expected from a pure TSI between two n orbitals relatively far apart; the n_+ level is lower than the n_- with very small energy splitting, $\Delta E=-0.19$ eV.

In the case (i) TBI is only possible over σ^* orbitals so that both levels are depressed, the n_- being depressed more than the n_+ so that the level order is reversed to n_- below n_+ with small ΔE value. When however TBI is allowed through σ only in the case (iii), both levels are elevated substantilly. In this case the elevation of n_+ is more than twice of the elevation of n_- level resulting in a large energy splitting of $\Delta E=4.98$ eV. This indicates that nearly 95 % of the total TBI is attributable to the interaction of n orbitals with bonds of σ framework. In the distorted structure, as a result of TBI, n_- is lowered only by 0.71 eV whereas n_+ is elevated as much as 8.76 eV. This is a natural consequence of narrow energy gap between n and HO-σ of the σ framework (Table 1) and the greater overlap between n and σ compared to that between n and σ^* (Table 4).

For the structure D, it can be seen that the effect of eliminating σ is entirely on n_+ whereas that of σ^* is on n_-. The results for the structure E, on the other hand, indicates that due to a drastic reduction of the n_+ elevation effect, the level ordering is reversed to n_+ below n_- level[9]. Here again the main cause of this level order reversal is the elimination of bond (σ) orbitals; elimination of σ^* alone does not cause appreciable difference from that of the structure D. The removal

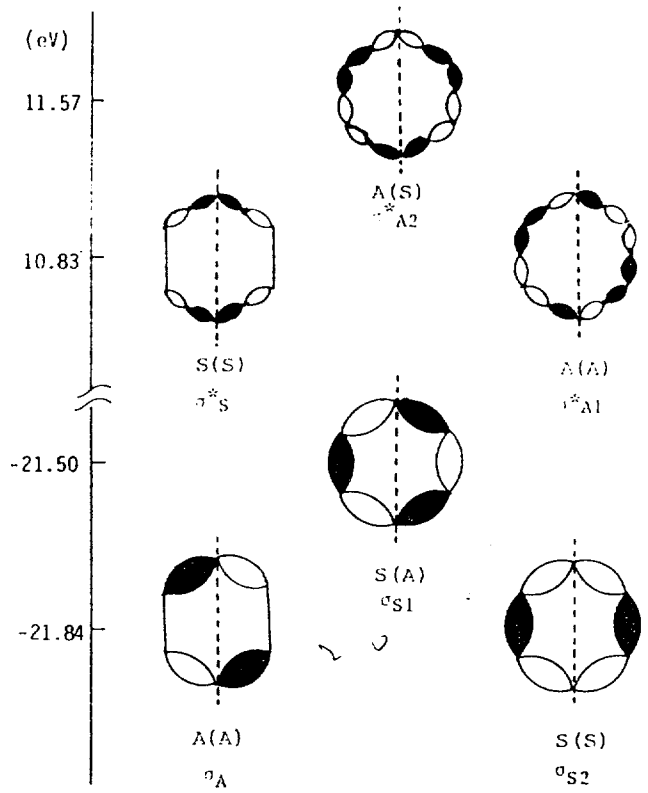

Figure 2. FMO Patterns of σ–framework for benzene: S and A refer to symmetric and antisymmetric with respect to the plane perpendicular to molecular axis in dotted lines, respectively. Symmetry notations in parenthesis are symmetries with respect to the plane along molecular axis. Orbital notations signify *e.g.* σ_{S1} and σ^*_S as the first symmetric σ and symmetric σ^* orbitials respectively.

of one side entirely from the molecule as in the structures F and G, causes no great change in the effect of $n-\sigma$ or $n-\sigma^*$ interaction relative to those in D, albeit TBI is somewhat greater in F compared with that in D.

It is however evident that TBI is more efficient *via* the distorted part (in G) than *via* the undistorted part (in F).

Finally we will examine LCBO–MOs of n_+ and n_- levels for various structures with σ or σ^* eliminated. We obtained FMO patterns of σ framework using benzene as a model by carrying out the LCBO calculations with all the C–H bond deleted.

The patterns correspond to those obtained by the "C–approximation". As shown in Figure 2, the HOMOs and LUMOs form threefold degenerate (or near degenerate) levels. The HO-σ and LU-σ^* for the structure B, where lone-pairs are removed from the framework, should give the same MO patterns. The LCBO–MO coefficients given in Table 7 confirms this correspondence.

If we were to place n orbitals on the two carbons, or N atoms as in pyrazine, on the molecular axis shown by dotted lines, the symmetry with respect to the plane perpendicular to this axis should be the one to be considered in conjunction with the symmetry of the $n_\pm$ orbitals.

Since only orbitals with the same symmetry are allowed to interact, the two levels can be expressed as,

$$n_+(S)=a_1(n_1+n_2)+a_2\sigma_{S1}+a_3\sigma_{S2}+a_4\sigma^*_S \qquad (2)$$

TABLE 7: LCBO-MO Coefficients for n_+ and n_- Orbitals of Various Partially Eliminated Structures

$n_\pm = C_1(n_1 \pm n_2) + C_2\sigma_{23} + C_3\sigma_{56} + C_4(\sigma_{12} \pm \sigma_{34}) + C_5(\sigma_{16} \pm \sigma_{45}) + C_6\sigma_{23}^* + C_7\sigma_{56}^* + C_8(\sigma_{12}^* \pm \sigma_{34}^*) + C_9(\sigma_{16}^* \pm \sigma_{45}^*)$

			C_1	C_2	C_3	C_4	C_5	C_6	C_7	C_8	C_9
A		n_+^{00}	0.468	−0.495	0.241	−0.171	−0.183	0.000	0.000	−0.025	−0.073
		n_-^{00}	0.627	0.000	0.000	0.218	−0.103	0.092	−0.079	−0.030	0.059
B	$\alpha=120$	HO-σ	0.000	0.398	−0.398	0.187	−0.187	0.000	0.000	0.038	0.038
		LU-σ^*	0.000	0.000	0.000	0.029	−0.029	0.349	0.350	−0.180	−0.179
	$\alpha=90$	HO-σ	0.000	0.696	−0.213	0.036	−0.226	0.000	0.000	0.021	0.047
		LU-σ^*	0.000	0.000	0.000	−0.021	0.019	0.047	0.136	0.259	−0.236
C	σ	n_+	0.703	0.000	0.000	0.000	0.000	0.000	0.000	−0.019	−0.043
		n_-	0.699	0.000	0.000	0.000	0.000	0.104	−0.078	−0.014	0.031
	$\sigma+\sigma^*$	n_+	0.707								
		n_-	0.707								
	σ^*	n_+	0.482	0.486	0.238	−0.172	−0.199	0.000	0.000	0.000	0.000
		n_-	0.638	0.000	0.000	−0.204	−0.111	0.000	0.000	0.000	0.000
D	σ	n_+	0.501	0.000	0.468	−0.183	−0.114	0.000	0.000	−0.051	0.031
		n_-	0.629	0.000	0.000	−0.210	−0.089	0.092	−0.080	−0.037	0.052
	$\sigma+\sigma^*$	n_+	0.501	0.000	0.468	−0.183	−0.114	0.000	0.000	−0.051	0.031
		n_-	0.640	0.000	0.000	−0.213	−0.128	0.000	−0.081	−0.028	0.050
	σ^*	n_+	0.469	0.495	0.241	−0.165	−0.189	0.000	0.000	−0.031	0.067
		n_-	0.640	0.000	0.000	−0.213	−0.128	0.000	−0.081	−0.028	0.050
F	σ	n_+	0.512	0.000	0.478	0.000	0.223	0.000	0.000	−0.044	0.023
		n_-	0.438	0.000	0.000	0.000	−0.405	0.122	−0.041	−0.003	−0.024
	$\sigma+\sigma^*$	n_+	0.516	0.000	0.472	0.000	−0.233	0.000	0.000	−0.003	−0.024
		n_-	0.491	0.000	0.000	0.000	−0.406	0.000	−0.047	0.000	0.023
	σ^*	n_+	0.473	0.488	0.243	−0.164	−0.196	0.000	0.000	0.000	0.067
		n_-	0.633	0.000	0.000	−0.224	−0.104	0.000	−0.083	0.000	0.053

$$n_-(A) = a_1'(n_1 - n_2) + a_2'\sigma_{A1}^* + a_3'\sigma_{A2}^* + a_4'\sigma_A \qquad (3)$$

where coefficients a_i and a_i' are mixing coefficients given by the perturbation theory as a form $\frac{H}{\Delta\varepsilon} \cong \frac{kS}{\Delta\varepsilon}$; thus the smaller the energy gap, and the larger the overlap, between two interacting orbitals, the greater the mixing. Based on these, we can immediately arrive at the following qualitative conclusions, which are indeed substantiated as shown in Table 7.

$$\left.\begin{array}{l} a_1 > a_2 > a_3 \gg a_4 \\ a_1' > a_4' > a_2' > a_3 \end{array}\right\} \text{ from energy gap, (Figure 2).}$$

and in general, $a_i > a_i'$, from overlap, (Table 4). We now see why both n_+ and n_- can interact with both HO-σ and LU-σ^* in pyrazine (N=odd system) in contrary to the rules tabulated (for chain compounds) in Table 1; due to degenerate FMOs involved in ring compounds (Figure 2), $n_+(S)$ can interact with one of the LU-σ^* which has S symmetry and $n_-(A)$ with one of the HO-σ of framework which has A symmetry as given in eqns (2) and (3).

Table 7 shows that the contribution of σ_{23} increases dramatically while that of σ_{56} decreases as a result of bond angle distortion at the carbons 2 and 3 in the HO-σ framework MO (entry B). The interaction of n_+ with the HO-σ will thus be enhanced since the increase in σ_{23} will increase the vicinal overlap between the two orbitals.

It is interesting to note that the elimination of σ in the structure D and F brings about an enhanced contribution of σ_{A1}^* MO, *i.e.*, increase in a_2', in the n_- orbital so that n_- level is lowered to the level of structure A where no elimination is involved. When however σ^* is eliminated from D, n_+ level is fully restored to that of structure A, but σ^* elimination from F does not restore the n_+ level to that of structure A. This indicates that the σ_{23} (in D) is included in σ_S orbitals but not in σ_S^* orbital (Figure 2) which also mixes in to n_+ level in eq (2).

We therefore conclude that although there is some mixing of HO-σ into n_- and of LU-σ^* into n_+ due to σ_A and σ_S^* (Figure 2), the main interactions are those between n_+ and HO-σ and between n_- and LU-σ^* as was found for chain compounds in Table 1.

Acknowledgements. We thank the Ministry of Education and the Korea Research Center for Theoretical Physics and Chemistry for support of this work.

References

(1) I. Lee, *Bull. Korean Chem. Soc.*, **3**, 140 (1982); *Bull. Inst. Basic Sci.* (Inha Univ.), **4**, 25 (1983); *Tetrahedron*, **39**, 2409 (1983).

(2) H. J. Dewey, R. D. Miller and J. Michl, *J. Amer. Chem. Soc.*, **104**, 5298 (1982).

(3) M. J. S. Dewar, R. C. Bingham and D. H. Lo, MINDO/3, No. 308, QCPE, Indiana Univ. (1975); R. C. Bingham, M. J. C. Dewar and D. H. Lo, *J. Amer. Chem. Soc.*, **97**, 1285 (1975).

(4) (a) J. P. Foster and F. Weinhold, Univ. of Wisconsin Theor. Chem. Inst. Report WIS-TCI-626; (b) F. Weinhold and T. K. Brunck, *J. Amer. Chem. Soc.*, **98**, 3745 (1976).

(5) S. Alexandratos, "GAUSSIAN-70: The write up" 1976 (QCPE program No. 236)
(6) (a) R. A. Finnegan, *J. Org. Chem.*, **30**, 1333 (1965); (b) A. Streitwieser, Jr., G. R. Ziegler, P. C. Mowery, A. Lewis and R. G. Lawler, *J. Amer. Chem. Soc.*, **90**, 1357 (1968); (c) R. P. Thummel, *Acc. Chem. Res.*, **13**, 70 (1980); (d) R. Homann, *Acc. Chem. Res.*, **4**, 1 (1971).
(7) (a) T. K. Brunck and F. Weinhold, *J. Amer. Chem. Soc.*, **101**, 1700 (1979); *J. Amer. Chem. Soc.*, **98**, 4392 (1976); (b) P. A. Christiansen and W. E. Palke, *Chem. Phys. Lett.*, **31**, 462 (1975); (c) R. Hoffmann, A. Imamura and W. J. Hehre, *J. Amer. Chem. Soc.*, **90**, 1499 (1968). (d) N. D. Epiotis, R. L. Yate's, J. R. Larson, C. R. Kirmaier and F. Bernardi, *J. Amer. Chem. Soc.*, **99**, 8379 (1977).
(8) (a) A. Gavezzotti and L. S. Bartell, *J. Amer. Chem. Soc.*, **101**, 5142 (1979); (b) J. Tyrrell, R. B. Weinstock and F. Weinhold, *Int. J. Quantum Chem. XIX*, 781 (1981).
(9) M. Ohsak, A. Imamura and K. Hirao, *Bull. Chem. Soc. Japan*, **51**, 3443 (1978).

Superplastic Deformation in the Low Stress Region

Chun Hag Jang†, Chang Hong Kim and Taikyue Ree

Department of Chemistry, Korea Advanced Institute of Science and Technology, P. O. Box 150 Cheongyangni, Seoul 131, Korea *(Received December 8, 1983)*

Superplastic alloys generally exhibit a three-stage sigmoidal varition of stress (f) with strain rate ($\dot{s}$), the stages being named region 1, 2 and 3 according to the increasing order of stress or strain rate. In the recent years, two different types of papers have been published on the plastic deformation of Zn-22% Al eutectoid in region I differing in strain-rate sensitivity m ($=d\ln f/d\ln \dot{s}$). In this paper, the data of the two groups have been analysed by applying Kim and Ree's theory of superplastic deformation. (1) We obtained the paramteric values of X_{gi}/α_{gj} and β_{gj} (g: grain boundary, $j=1,2$ indicating flow units) appearing in Kim and Ree's theory [Eq. (2a)]. (2) It was found that the value of X_{g2}/α_{g2} is small for the group data with small m, *i.e.*, α_{g2}, which is proportional to the size of flow unit $g2$, is large whereas α_{g2} is small for the groups data with large m, *i.e.*, the size of the flow unit $g2$ is small. In other words, the two types of behavior occur by the size difference in the flow units. (3) From the β_{gj} value, which is proportional to the relaxation time of flow unit gj, the ΔH^{*}_{gj} for the flow process was calculated, and found that ΔH^{*}_{g2} is large for the group data with small m whereas it is small for the group data with large m. (4) The flow-unit growth was studied, but it was concluded that this effect is not so important for differentiating the two groups.(5) The difference in α_{g2} and in the growth rate of flow units is caused by minute impurities, crystal faults, *etc.*, introduced in the sample preparation.

1. Introduction

Superplastic alloys generally exhibit a three-stage sigmoidal curve in the plot of log f (stress) *vs.* log $\dot{s}$ (strain rate). The Zn-22 % Al eutectoid is one of the best known superplastic alloys, and many studies have been carried out on this alloy.[1~8] Experiments on Zn-22 % Al eutectoid alloys have revealed marked differences in the low stress region 1 so that the published data are divided into two distinct types as shown in Figure 1. In Figure 1 curve A shows a normal sigmoidal type of superplastic deformation,[1,3~6] while curve B does not,[2,7,8] that is, curve B has a higher strain-rate sensitivity ($m=d\ln f/d\ln \dot{s}$) than curve A over the range of low stresses, region 1. In spite of this obvious discrepancy in the strain-rate sensitivity, the two plastic deformations in the low stress region 1 show the same type of flow curves as will be shown later. In this paper much interests are paid on the superplastic deformation in the low stress region 1, and the behavior of superplastic deformation are analyzed according to the Kim-Ree theory.[9] The reason for the appearance of the two different types mentioned above will be clarified.

2. Theory

(*a*) *Analysis of Flow Curves.* According to the Ree-Eyring theory,[10~12] the relation between stress and strain rate for dislocation movements are expressed as the following:

$$f=f_d=\sum_{i=1}^{m}\frac{X_{di}}{\alpha_{di}}\sinh^{-1}(\beta_{di}\dot{s}_d) \tag{1a}$$

and

$$\dot{s}_d=\left(\frac{\lambda}{\lambda_1}2k'\right)_{di}\sinh\left[\left(\frac{\lambda\lambda_2\lambda_3}{2kT}\right)_{di}f_{di}\right] \tag{1b}$$

$$=(\beta_{di})^{-1}\sinh(\alpha_{di}f_{di}) \tag{1c}$$

where

$$\alpha_{di}\equiv\left(\frac{\lambda\lambda_2\lambda_3}{2kT}\right)_{di} \tag{1d}$$

and

$$(\beta_{di})^{-1}\equiv\left(\frac{\lambda}{\lambda_1}2k'\right)_{di} \tag{1e}$$

Here, the subscript d represents dislocation, f is the total stress applied on a dislocation slip plane, f_{di} is the stress acting on the ith kind of dislocation flow units, X_{di} is the